# The Effect of Polyelectrolyte Adsorption on Inter-Colloidal Forces

Itamar Borukhov and David Andelman\*
School of Physics and Astronomy,
Raymond and Beverly Sackler Faculty of Exact Sciences,
Tel-Aviv University, Ramat-Aviv 69978, Tel-Aviv, Israel

### Henri Orland

Service de Physique Théorique, CE-Saclay, 91191 Gif-sur-Yvette Cedex, France (September 9, 2021)

The behavior of polyelectrolytes between charged surfaces immersed in semi-dilute solutions is investigated theoretically. A continuum mean field approach is used for calculating numerically concentration profiles between two electrodes held at a constant potential. A generalized contact theorem relates the inter-surface forces to the concentration profiles. The numerical results show that over-compensation of the surface charges by adsorbing polyelectrolytes can lead to effective attraction between equally charged surfaces. Simple scaling arguments enable us to characterize qualitatively the inter-surface interactions as function of the fraction of charged monomers p and the salt concentration  $c_b$ . In the low salt regime we find strong repulsion at short distances, where the polymers are depleted from the inter-surface gap, followed by strong attraction when the two adsorbed layers overlap. The magnitude of this attraction scales as  $p^{1/2}$  and its dominant length scale is proportional to  $a/p^{1/2}$ , where a is the monomer size. At larger distances the two adsorbing surfaces interact via a weak electrostatic repulsion. For strong polyelectrolytes at high salt concentration the polymer contribution to attraction at short distances scales as  $p/c_b^{1/2}$  and the length scale is proportional to  $\kappa_s a^2/p$ , where  $\kappa_s^{-1}$  is the Debye-Hückel screening length. For weak polyelectrolytes at high salt concentration the interaction is repulsive for all surface separations and decays exponentially with a decay length equal to  $\kappa_s^{-1}$ . The effect of irreversible adsorption is discussed as well and it is shown that inter-surface attraction can be obtained in this case as well.

61.25.H, 68.10, 36.20, 41.10D

# I. INTRODUCTION

Polymers are known to affect the interactions of colloidal particles in solution [1–3]. Adsorption of charged polymers (polyelectrolytes) to oppositely charged colloids may turn inter-colloidal repulsion into attraction, leading to flocculation. This phenomenon is used in industrial applications such as water filtration, paper making and mineral processing. The reversed process is useful as well, since adsorbed polyelectrolytes (in different conditions) can also stabilize colloidal suspensions such as paint, ink or medical suspensions against attractive forces (e.g., van der Waals forces).

One of the most common techniques to study experimentally the adsorption of polyelectrolytes between two surfaces is the Surface Force Apparatus (SFA) [4], which allows delicate measurements of inter-surface forces at distances as small as a few Angstroms. In these experiments [5–12], attractive and repulsive forces have been observed, depending on specific details, such as the type of polyelectrolyte, its concentration, the ionic strength of the solution, etc. In other experiments it is possible to measure the disjoining pressure of thin liquid films in the presence of polyelectrolytes and as a function of the film width [13]. Both repulsive and attractive forces have been measured using this method.

Adsorption of polyelectrolytes was treated theoretically in a discrete model [14–17], where the state of the system is described by occupation fractions of monomers, ions and solvent molecules on a discrete lattice. Within mean field,

the equilibrium state of the system corresponds to the maximal contribution to the partition function of the system, and can be calculated numerically. Böhmer et al. [18] have used this model to calculate force curves at relatively short distances (up to 30 molecular layers). In addition, Monte Carlo computer simulations of polyelectrolytes between flat surfaces [19] and between charged spheres [20] provide valuable hints concerning the complex behavior of polyelectrolytes. However, they are limited to relatively short chains and small inter-surface distances due to computation time limitations.

Another theoretical approach is a continuum one [21–28] where the concentration of the different species are taken to be continuous functions of the spatial coordinates. The mean–field state can be calculated by solving two differential equations for the polymer concentration and the electrostatic potential derived using a variational procedure. Varoqui et al. [22,23] used the continuum approach to investigate polyelectrolyte adsorption onto one surface, while Podgornik [27] used a similar formalism to calculate inter–surface forces. In those works the non-linear excluded volume interaction between the monomers has not been considered. Châtellier and Joanny [28] used a linearized version of a similar approach to study the inter–surface interactions for polyelectrolytes in a poor solvent. Recently, we have been able to derive some simple scaling relations for the adsorption of polyelectrolytes onto a single charged surface [26]. These scaling relations were compared to the exact numerical solutions of the differential equations and to existing experimental results. The agreement was reasonable in two opposite limits: (i) low salt concentration (no electrostatic screening) and (ii) high salt concentration (strong screening).

In the present work, the continuum model is used to study polyelectrolyte adsorption between two parallel surfaces. The advantage of our model is that the connectivity of the polymer chains, the excluded volume repulsion between monomers in a good solvent and the Coulomb interactions between the charged monomers, counter-ions, co-ions and surface charges are all taken into account. The mean field equations are solved numerically in order to obtain concentration profiles, and the inter-surface interactions are then calculated from the free energy. In addition we extend our earlier scaling approach of one adsorbing surface [26] to the case of two interacting surfaces. The result is a qualitative description of the inter-surface interactions as function of the polyelectrolyte charge and the amount of salt in the solution.

The paper is organized as follows: in the next section we describe the mean-field approach. In Sec. III we present numerical results obtained from solving the mean field equations, and in Sec. IV we use simple scaling arguments to describe the inter-surface interactions. In Sec. V we study the effect of irreversible adsorption both numerically and analytically and in Sec. VI we compare our results with experiments. Finally we present our conclusions and some future prospects.

## II. THE MEAN FIELD APPROACH

### A. The Basic Equations

The model system consists of a semi-dilute solution of polyelectrolytes in a good solvent placed between two flat surfaces (Fig. 1). The solution contains charged polymer chains, counter-ions and a monovalent electrolyte (salt). Having in mind the experimental setup of the surface force apparatus (SFA) discussed below, we consider a system

which is coupled to a bulk reservoir of polyelectrolyte chains and salt.

As discussed elsewhere [24,25], the charge distribution along the chains depends on the type of polyelectrolyte as well as on the local conditions, such as the pH and the electrostatic potential. However, at low electrostatic potentials  $|\beta e\psi| \ll 1$ , where  $\psi$  is the electrostatic potential,  $\beta = 1/k_BT$  the inverse thermal energy and e the electron charge, the differences between the various charge distribution models are small. We therefore assume hereafter a uniform charge distribution along the polymer chains with a fractional charge pe attached to each monomer.

In the mean field approach, the free energy of the system is expressed in terms of the local electrostatic potential  $\psi(\mathbf{r})$  at a point  $\mathbf{r}$  and the polymer order parameter  $\phi(\mathbf{r})$  which is related to the local monomer concentration through  $c_m(\mathbf{r}) = |\phi(\mathbf{r})|^2$ . The relation between the polymer order parameter and the monomer concentration is analogous to the relation between the wave function and the probability density of a particle in quantum mechanics. The excess free energy with respect to the bulk can be divided into three contributions [22–25]:

$$F = \int f(\mathbf{r}) d\mathbf{r} = \int \left\{ f_{\text{pol}}(\mathbf{r}) + f_{\text{ions}}(\mathbf{r}) + f_{\text{el}}(\mathbf{r}) \right\} d\mathbf{r}$$
(1)

The polymer contribution is

$$f_{\text{pol}}(\mathbf{r}) = k_B T \left[ \frac{a^2}{6} |\nabla \phi|^2 + \frac{1}{2} v(\phi^4 - \phi_b^4) \right] - \mu_p(\phi^2 - \phi_b^2)$$
 (2)

where the first term is the polymer response to local variations of the concentration and is due to the connectivity of the polymer chain, a being the effective monomer size. The second term represents the short ranged monomer—monomer interaction and can be viewed as representing an effective volume of a single monomer. For a polymer in a good solvent v is positive. However, since v represents an effective monomer—monomer interaction it can also be negative (in a poor solvent) or zero (in a theta solvent) requiring higher order terms in  $\phi^2$  to be included in the free energy. For simplicity we will limit ourselves to good solvent conditions but the formalism can be easily generalized to other conditions as well. The last term couples the system to a reservoir,  $\mu_p$  being the polymer chemical potential and  $\phi_b^2$  the bulk monomer concentration.

The non–electrostatic contribution of the small (monovalent) ions is due to their translation entropy and is equal to

$$f_{\text{ions}}(\mathbf{r}) = \sum_{i=\pm} \left\{ k_B T \left[ c^i \ln c^i - c^i - \left( c_b^i \ln c_b^i - c_b^i \right) \right] - \mu^i \left( c^i - c_b^i \right) \right\}$$
(3)

where  $c^i(\mathbf{r})$  is the local concentration of the  $i=\pm$  ions (cations and anions) and  $c_b^i$ ,  $\mu^i$  are the bulk concentration and chemical potential, respectively. In the most general case the solution contains two types of negative ions: the counter-ions which dissociate from the polymer chains and the salt anions. In the reservoir the concentration of negative ions has two contributions  $c_b^- = c_b + p\phi_b^2$  where  $c_b$  is the electrolyte bulk concentration, while for the positive ions  $c_b^+ = c_b$ . In principle, one could consider the two types of negative ions separately, but for clarity we take the two types of negative ions to be identical.

Finally, the electrostatic contribution is

$$f_{\rm el}(\mathbf{r}) = pe\phi^2\psi + ec^+\psi - ec^-\psi - \frac{\varepsilon}{8\pi}|\nabla\psi|^2$$
(4)

The first term is the electrostatic energy of charged monomers. The next two terms represent the positive and negative ions, respectively, and the last term is the self energy of the electric field where  $\varepsilon$  is the dielectric constant of the solution. The sum of the electrostatic contributions can be integrated by parts using the Poisson equation (derived below) and yields  $F_{\rm el} = (\varepsilon/8\pi) \int |\nabla \psi|^2 d{\bf r}$ , as expected, plus electrostatic surface terms.

Minimization of the free energy with respect to  $c^{\pm}$ ,  $\phi$  and  $\psi$  yields a Boltzmann distribution for the concentration of the small ions,  $c^{\pm}(\mathbf{r}) = c_b^{\pm} \exp(\mp \beta e \psi)$ , and two coupled differential equations for  $\phi$  and  $\psi$  [25]:

$$\nabla^2 \psi(\mathbf{r}) = \frac{8\pi e}{\varepsilon} c_b \sinh(\beta e \psi) - \frac{4\pi e}{\varepsilon} \left( p \phi^2 - p \phi_b^2 e^{\beta e \psi} \right) \tag{5}$$

$$\frac{a^2}{6}\nabla^2\phi(\mathbf{r}) = v(\phi^3 - \phi_b^2\phi) + p\phi\beta e\psi \tag{6}$$

Equation 5 is a generalization of the Poisson–Boltzmann equation including the free ions as well as the charged polymers. The first term represents the salt contribution and the second term is due to the charged monomers and their counter-ions. Equation 6 is a generalization of the self–consistent field equation of neutral polymers [29]. In the bulk the potential and the polymer concentration have constant bulk values given by  $\psi = 0$  and  $\phi = \phi_b$ , as can be seen in the above equations.

### **B.** Two Interacting Surfaces

The interaction of two charged surfaces in a solution containing only small ions (electrolyte) without charged polymers is well established within the framework of the Poisson–Boltzmann equation [30]. The electrostatic interaction between two identically charged surfaces is found to be repulsive within this mean-field like theory [31]. However, the addition of polyelectrolytes to the solution changes the picture in a subtle way. Experiments [5–13] show that polyelectrolytes reduce this repulsion and might even cause mutual attraction between the two surfaces.

For simplicity, the surfaces are taken as flat, homogeneous and parallel to each other in order that the physical quantities will depend only on the position x between the surfaces (see Fig. 1). The effect of the surfaces is introduced through the boundary conditions on the polymer order parameter  $\phi(x)$  and the electrostatic potential  $\psi(x)$ . In this work, both surfaces are assumed to be kept at the same constant potential:

$$\psi|_{s} = \psi_{s} \tag{7}$$

and no monomers are adsorbed on the surfaces

$$\phi|_{s} = 0 \tag{8}$$

Other boundary conditions could have been considered as well. For example, if a fixed surface charge  $\sigma$  is assumed then the electrostatic boundary condition would include the electric field:  $\psi'|_s = -4\pi\sigma/\varepsilon$ . In real systems neither the surface potential nor the surface charge are fixed. The choice of one or another is only an approximation whose quality depends on the details of the experimental system. Similarly, for the polymer boundary conditions one could consider an adsorbing surface instead of a non-adsorbing one [33].

Given these boundary conditions, the Poisson–Boltzmann and self-consistent field equations (5,6) uniquely determine  $\psi(x)$  and  $\phi(x)$ . However, experiments usually probe global properties such as the amount of monomers adsorbed per unit area or the inter–surface interactions.

The total amount of monomers (per unit area) between the two surfaces  $\Gamma(w)$  can be easily calculated from the polymer concentration profile since

$$\Gamma(w) = \int_{-w/2}^{w/2} \phi^2(x) \mathrm{d}x \tag{9}$$

Another measure for the strength of the adsorption is the average monomer concentration divided by the bulk concentration:

$$\left\langle \frac{\phi^2}{\phi_b^2} \right\rangle = \frac{1}{w} \int_{-w/2}^{w/2} \frac{\phi^2(x)}{\phi_b^2} dx = \frac{\Gamma(w)}{w\phi_b^2} \tag{10}$$

The latter quantity relates to the strength of the adsorption only at small distances. As demonstrated by the numerical examples below, at larger distances,  $\Gamma$  saturates to a constant and the average concentration decreases as 1/w.

In addition, it is of interest to calculate the total amount of charge (per unit area) carried by the adsorbed polymers  $\sigma_p(w) = pe\Gamma(w)$  as compared to the induced surface charge density  $\sigma_s(w)$  (on a single surface). The latter depends on the inter-surface distance as we have chosen to work with constant surface potentials rather than constant surface charges.

The adsorption of polyelectrolytes strongly affects the inter-surface interactions. The excess free energy per unit area for two surfaces at a distance w apart can be calculated from the concentration profiles  $\phi(x)$  and  $\psi(x)$ :

$$\Delta F(w) = \int_{-w/2}^{w/2} f[\phi(x), \psi(x)] dx - 2F_1$$
 (11)

where f(x) was introduced in eqs. 1-4 and  $F(w \to \infty) = 2F_1$  is the free energy of two isolated surfaces at infinite separation.

The variation of this free energy with respect to the inter-surface distance w gives the inter-surface pressure (or force per unit area):

$$\Pi(w) = -\frac{\delta(\Delta F)}{\delta w} \tag{12}$$

It can be shown from eqs. 11,12 and from  $\delta(\Delta F)/\delta\phi(x) = \delta(\Delta F)/\delta\psi(x) = 0$  that

$$\Pi(w) = -f(x=0) \tag{13}$$

where f(x=0) is the free energy density (per unit volume) at the mid-plane. This relation is a generalization of the contact theorem of neutral polymers [34]. In our case the calculation of f(x=0) yields:

$$\beta\Pi(w) = -p\phi^2(0)y(0) - \frac{1}{2}v(\phi^2(0) - \phi_b^2)^2 + p\phi_b^2[e^{y(0)} - 1] + 2c_b[\cosh(y(0)) - 1]$$
(14)

where  $y(0) = \beta e \psi(0)$  is the reduced electrostatic potential at the symmetry plane (x = 0). The above expression is obtained by inserting the equilibrium (Boltzmann) distribution of the small ions  $c^{\pm} = c_b^{\pm} \exp(\mp \beta e \psi)$  back into the free energy, eqs. 2-4.

Equations 12 and 13 for the force are valid for the planar geometry (Fig. 1). In some experiments [13] where the disjoining pressure of thin liquid films is measured, the two surfaces are indeed parallel to each other and  $\Pi(w)$  is measured directly. However, most experiments [5–12] use the surface force apparatus [4] where the force  $\Pi_R$  is measured between two cylindrical surfaces of radii R with a 90° tilt between their major axes (see Fig. 2a). At small distances  $w \ll R$  the Derjaguin approximation [30] relates the measured force to the excess free energy (as given by eq. 11) and not to its derivative (as given by eqs. 12,13)

$$\frac{\Pi_R(w)}{R} = 2\pi\Delta F(w) \tag{15}$$

For clarity purposes we denote the force per unit area acting between two infinite flat surfaces as  $\Pi(w)$  (eqs. 12,13), and the absolute force acting between two cross cylinders as  $\Pi_R(w)$ .

The Derjaguin approximation can also be used to calculate the interaction between two spheres of radii R at small distances  $w \ll R$  (Fig. 2b) as is the case for colloidal suspensions. The inter-colloidal force is related to the interaction free energy of two flat surfaces but with a different numerical factor:

$$\frac{\Pi_R(w)}{R} = \pi \Delta F(w) \tag{16}$$

### III. NUMERICAL RESULTS

### A. Low Salt Concentration

Concentration Profiles: In order to solve the mean-field equations (eqs. 5,6), we use a minimal squares scheme in which the spacing between the two surfaces is divided into  $N \sim 100$  intervals. An error functional which sums the squares of the local errors in eqs. 5,6 is minimized with respect to the values of  $\phi$  and  $\psi$  at the discrete grid points, under the constraint of the boundary conditions eqs. 7,8.

Typical solutions are presented in Fig. 3. The polymer is positively charged (p=1) and attracted to non-adsorbing surfaces held at a constant negative potential  $(\psi_s < 0)$ . Here we focus on the weakly screened limit (low salinity). The effect of screening can be estimated by comparing the inter–surface separation w with the Debye–Hückel screening length  $\kappa_s^{-1}$  defined by  $\kappa_s^2 = 8\pi l_B c_b$  where  $l_B = e^2/\varepsilon k_B T$  is the Bjerrum length equal to 7Å for aqueous solutions at room temperature. At low salt concentration,  $\kappa_s^{-1} \gg w/2$ , screening is weak and plays only a minor role, whereas at high salt concentration,  $\kappa_s^{-1} \ll w/2$ , screening strongly reduces the Coulomb interactions in the adsorbed layer. In Fig. 3, the solution contains a small amount of monovalent salt  $(c_b = 1 \text{mM})$  so that the electrostatic screening length  $\kappa_s^{-1} \simeq 100\text{Å}$  is larger than the inter–surface distance which varies between 7 and 40Å.

In Fig. 3a the reduced electrostatic potential  $y(x) = \beta e \psi(x)$  is plotted as a function of the position x between the two surfaces. The reduced monomer concentration  $\phi^2(x)/\phi_b^2$  is shown in Fig. 3b. Despite the fact that the surface potential is not very high,  $y_s = -2.0$  corresponding to  $\psi_s \simeq -50 \text{mV}$ , the adsorption is quite strong and the concentration in the gap between the two surfaces can increase by three orders of magnitude above the bulk concentration. The adsorption here is purely electrostatic since the only source of attraction is due to the electrostatic boundary conditions. A neutral polymer in similar conditions will not adsorb to the surfaces.

At small inter–surface distances the adsorbed polymers consist of a single layer extending from one surface to the other and the potential is negative everywhere in the gap. As the surfaces are drawn away from each other, first the amount of adsorbed polymer grows rapidly and then the adsorbed layer separates into two distinct layers near the two surfaces. In addition, the potential changes sign and becomes positive in the central region. By integrating the Poisson equation from the surface to the point where the potential changes sign, it can be easily shown that this sign reversal is due to an over–compensation of the surface charges by the layer of adsorbed monomers.

The over–compensation is specific to charged polymers and does not appear in the Poisson-Boltzmann formalism for small ions (regular electrolytes). Physically, charged monomers which adsorb close to the surface are connected to other monomers which reside at some larger distance. In our model, the polymer chains resist fluctuations on length scales smaller than the Edwards correlation length  $\xi_E \sim a/\sqrt{vc_m}$  of neutral polymers and thus over–compensate the surface charges and cause the potential to reverse sign. This over-compensation is much more pronounced when salt is added to the solution as will be discussed below. In the central region where the sign of the potential is opposite to that of the surface potential, the concentration of negative ions is larger than that of positive ions. We stress that when all contributions to the charge density are considered (polymer and small ions), the charges in the solution exactly balance the surface charges (see Fig. 5).

At yet larger distances (w > 20Å for the physical parameters of Fig. 3) the two adsorbed layers do not change any more. This occurs when the inter–surface distance w is larger than twice the width of the adsorbed layers. The two surfaces are almost decoupled and single surface adsorption is recovered. The polymer concentration between the two adsorbed layers is small and comparable to the bulk concentration. As long as the screening length  $\kappa_s^{-1}$  is larger than the distance w, the electrostatic potential is nearly a constant (e.g.  $y \simeq 0.2$  in Fig. 3). At even larger distances,  $w > \kappa_s^{-1}$ , the effect of screening will show up, and the mid–plane potential will gradually decay to zero.

Polyelectrolyte Adsorption: In Fig. 4a the total amount of monomers (per unit area) adsorbed between the two surfaces  $\Gamma(w)$  is plotted as a function of the inter-surface distance w for two charge fractions p=1 (solid curve) and p=0.2 (dashed curve). Similarly, in Fig. 4b the average reduced monomer concentration  $\langle \phi^2/\phi_b^2 \rangle$  is plotted as a function of w. Three regimes can be distinguished in accord with the findings presented on Figs. 3-4: at very short distances ( $w \simeq 5\text{Å}$ ) the confinement of the polymer to a narrow slit competes with the electrostatic attraction of the charged monomers to the surface and avoids strong adsorption. The polymer is not expelled totally from the gap between the two surfaces but its concentration is of the order of the bulk concentration.

As the surfaces are taken further apart, the adsorption increases rapidly until it reaches its maximal value. At this point the average concentration can be three orders of magnitude higher than the bulk concentration. At larger distances the two surfaces decouple from each other and the adsorbed amount decreases towards a saturation value. At this stage the system can be described as two independent layers adsorbing onto the two surfaces. The saturation value of  $\Gamma$  is approximately twice the adsorbed amount to a single surface  $\Gamma(w \to \infty) = 2\Gamma_1$ . In a preceding work [26] we investigated adsorption onto a single surface and have shown that in the low salt limit  $\Gamma_1 \sim 1/\sqrt{p}$ . This behavior is a result of two competing interactions: (i) the electrostatic attraction of the charged monomers to the surface which is proportional to p; and (ii) the Coulomb repulsion between charged monomers in the adsorbed layer which is proportional to  $p^2$ . For strong polyelectrolytes the latter interaction dominates and the adsorbed amount  $\Gamma_1$ 

increases as the fractional charge p decreases. This scaling behavior is in accord with the saturated values of Fig. 4a. In Fig. 5 the charge densities per unit area are plotted as functions of the distance w for the same sets of values as in Fig. 4. Using the single surface results we verify that indeed in the saturated regime of large inter-surface separations  $\sigma_p(\infty) \sim p\Gamma_1 \sim \sqrt{p}$ . Another observation which can be made from Fig. 5 is that the two charge densities almost balance each other. In the low salt limit these charge densities must cancel each other since the amount of salt is too small to play any significant role in neutralizing the solution.

Free Energies and Forces: In Fig. 6, inter-surface force profiles were calculated for  $c_b = 10^{-6}$ M, corresponding to  $\kappa_s^{-1} \simeq 3000$ Å, and for two values of the polymer charge fraction p. In Fig. 6a, the excess free energy per unit area  $2\pi\Delta F(w)$ , eq. 11, which is the physical quantity measured in SFA experiments, is plotted as a function of the inter-surface distance w. In Fig. 6b the force per unit area  $\Pi(w)$ , eq. 12, acting between flat surfaces is plotted as a function of the distance. This force can be measured directly in disjoining pressure experiments of thin films [13].

The two surfaces strongly repel each other at very short distances and attract at short distances. Note that for small ions such attraction is not present within the Poisson-Boltzmann approximation. For polymer chains the lack of translational entropy as well as the large correlation length  $\xi_E$  enhance the effective attraction between the surfaces at short separations. As the charge fraction is lowered, the attraction becomes weaker and the length scale of attraction increases. These two effects can be explained by simple arguments which are presented in section IV. Attractive interactions have been observed experimentally [8] and were attributed to "bridging" of chains between the surfaces—a mechanism which is not present in our approach.

A secondary repulsion appears at large distances but is too weak to be shown on a linear scale in our plots. However, this secondary repulsion can be made quite pronounced, in particular when the polymer surface excess is fixed at a large value. This is further discussed in Sec. V. For small ions, the origin of the repulsion is entropic whereas here it is due to over-compensation of the surface charges.

# B. High Salt Concentration

Concentration Profiles: At high salt concentration the screening length  $\kappa_s^{-1}$  is smaller than the inter–surface separation w. The effect of screening on the concentration profiles is demonstrated in Figs. 7 and 8, where a strong polyelectrolyte (p=1) is adsorbed from a solution containing large amounts of salt,  $c_b = 1$ M for which the screening length is  $\kappa_s^{-1} = 3$ Å. In Fig. 7 the reduced electrostatic potential and the reduced monomer concentration are plotted as function of the position x for a range of inter-surface distances w. As a result of screening the attraction of charged monomers to the surface is reduced considerably as compared to the low salt limit and the total amount of adsorbed polymer is approximately half. Despite the weaker adsorption, the qualitative behavior is similar. At short distances ( $w \lesssim 15$ Å in Fig. 7b) a single adsorbed layer exists between the two surfaces. At intermediate distances (15Å  $v \lesssim 40$ Å) this layer separates into two strongly interacting layers and at larger distances ( $w \gtrsim 40$ Å) the two layers decouple from each other and only weakly interact with each other.

When the separation is large enough ( $w \gtrsim 15\text{Å}$  in Fig. 7) the adsorption is strong enough so that the charged polymer over–compensates the surface charges. The signature of this effect is that the electrostatic potential changes sign in the

central region as seen in Fig. 7a. This sign reversal strongly affects the small ion concentration  $c^{\pm}(x)$  as demonstrated in Fig. 8. Since the concentration of the small ions follows a Boltzmann distribution  $c^{\pm}(\mathbf{r}) = c_b^{\pm} \exp(\mp \beta e \psi)$  the concentration of small negative ions  $c^{-}$  in the central region exceeds that of the positive ions  $c^{+}$  as can be seen in Fig. 8 for w = 40Å (solid curve). Altogether, the net charge (per unit area) in the central region will be negative ensuring an overall charge neutrality between the two surfaces. Note, that at small separations (e.g. w = 10Å in Fig. 8) the potential is negative everywhere and the concentration of positive ions exceeds that of the negative ions everywhere within the gap.

Polyelectrolyte Adsorption: Despite the effect of screening, the adsorption of strongly charged polyelectrolytes is strong as can be seen in Fig. 7b. The reason is that screening has two competing effects: on one hand it reduces the attraction of charged monomers to the surface which is the driving force for adsorption. On the other hand screening also reduces the monomer-monomer Coulomb repulsion between adsorbed monomers, thus allowing for more charges to accumulate near the surface. Hence, despite the fact that the range of the electrostatic interaction is reduced considerably, the average polymer concentration near the surface can be high (as long as p is not too small).

In contrast with the low salt regime, here the small ions play an important role in balancing the surface charges. In Fig. 9 the different contributions to the charge densities per unit area are plotted as function of the distance w. The negative curve corresponds to the (induced) surface charge density on the two surfaces  $2\sigma_s$ . The positive curves correspond to the total amount of polymer charges  $\sigma_p$  (per unit area) which have adsorbed between the two surfaces, and the total amount of charge carried by small ions  $\sigma^+ + \sigma^-$ . At short distances,  $w \lesssim 6\text{Å}$ , the polymer contribution is small and the main contribution to the charge density is that of the small ions. This distance can also be regarded as a lower cutoff to the continuum theory employed here since the monomer size we employed is of the same order of magnitude (a = 5Å).

When the surfaces are taken further apart, the polymer contribution and the net contribution of the small ions saturate to a constant value. This occurs when the two adsorbing surfaces decouple from each other, and two distinct adsorbed layers build up on each of the surfaces. Unlike the low salt case where the contribution of the small ions is negligible and the charged polymers dominate the charge density, in the high salt regime the contributions of the small ions and the polymer are comparable in magnitude. For example, in Fig. 9, the polymer contributes about one third of the charge density (per unit area) between the surfaces while the small ions contribute the other two thirds.

Free Energies and Forces: Screening has a pronounced effect on the inter–surface interactions as can be seen in Fig. 10, where the inter–surface interactions are plotted as function of the distance for a strong polyelectrolyte (p = 1) at high salt concentration. The general behavior here is similar to the low salt case as is seen in Fig. 6. As the amount of salt increases, the adsorption is reduced because of the electrolyte screening and the attractive forces become substantially weaker. Similar effects were also observed experimentally in SFA experiments [8,11].

Since the forces are related to the mid-plane values of  $\psi$  and  $\phi$  (eq. 12), it is of interest to study the mid-plane values of  $\psi(0)$ . In the inset of Fig. 10 the mid-plane value of the reduced electrostatic potential  $y(0) = \beta e \psi(0)$  is plotted as a function of the inter-surface distance for the same profiles that are used in the calculation of the forces. As can be seen also in Figs. 3 and 7, the mid-plane potential is negative at short distances, changes sign to become positive and finally decays to zero. The inter-surface interaction changes from repulsion to attraction at about the same distance

where the mid-plane electrostatic potential changes sign. This observation can be explained by examining the various contribution to the local free energy at the mid-plane, eqs. 2-4. At the mid-plane the squared gradient terms in  $\phi$  and  $\psi$  vanish. In addition, for strong polyelectrolytes the excluded volume and chemical potential terms are very small. The force  $\Pi(w) = -f(x=0)$  is dominated by two terms.

$$\beta \Pi \simeq -p\phi^2(0)y(0) + 2c_b \left[\cosh(y(0)) - 1\right] \tag{17}$$

The first term is the contribution of the charged monomers and changes sign when y(0) changes sign. The second is the (repulsive) osmotic pressure of the small ions and is proportional to  $y^2(0)$  at small values of y(0). It is clear from the above that as long as the mid-plane potential is small enough,  $y(0) \ll p\phi^2(0)/c_b$ , the pressure is governed by the first term and will change sign from attraction to repulsion when y(0) changes sign. It now follows that for a positively charged polymer, negative (positive) mid-plane potentials lead to repulsion (attraction) in agreement with Fig. 10. Since the potential changes sign when the adsorbed monomers over-compensate the surface charge, we conclude that this over-compensation is responsible for the reversal in the sign of the interaction.

Weak polyelectrolytes ( $p \ll 1$ ) do not adsorb as much as strong polyelectrolytes. The attractive forces are much weaker and are easily overpowered by the double layer repulsion of the small ions. Such an example is presented in Fig. 11, where the inter–surface forces are calculated for a low charge fraction (p = 0.1) at two high salt concentrations  $c_b = 0.25$ M and  $c_b = 1$ M. In contrast with the case of strong polyelectrolytes, here the forces are repulsive over the whole distance range and decay on a length scale of  $\kappa_s^{-1}$ .

### IV. SCALING REGIMES

The fundamental difficulty in studying polyelectrolytes is due to the competition between short range interactions such as the chain elasticity and excluded volume interactions, and the long range electrostatic interactions. In a previous work [26] we have studied polyelectrolyte adsorption to a single surface by separating the two competing length scales: (i) The adsorption length D, which characterizes the width of the adsorbed layer and (ii) the electrostatic screening length  $\kappa_s^{-1} = (8\pi l_B c_b)^{-1/2}$  assuming that  $c_b \gg p\phi_b^2$ . The screening length depends on the salt concentration, while the adsorption length depends on both electrostatic and non-electrostatic properties.

The two length scales can be separated in two limits: (i) the low salt regime  $D \ll \kappa_s^{-1}$  and (ii) the high salt regime  $D \gg \kappa_s^{-1}$ . The difference between the two regimes being the range of the electrostatic interactions. The main assumption in this approach is that the polymer profile near a single flat surface can be written in the form

$$\phi(x) = \sqrt{C} \ h\left(\frac{x}{D}\right) \tag{18}$$

where h(z) is a dimensionless function normalized to unity at its maximum and C sets the scale of polymer adsorption. The free energy can then be expressed in terms of D and C while the exact form of h(z) affects only the numerical prefactors. Minimization of the free energy with respect to D and C gives the single surface adsorption length  $D_1$  and the concentration scale  $C_1$ .

When two surfaces interact with each other, the single surface profile is affected by the presence of the other surface. As a result the shape of the profile changes with the separation w as demonstrated in Figs. 3 and 7. For example,

at short distances the profile varies monotonically between the surface and the half plane, while at larger distances it becomes non-monotonous, until finally the two surfaces decouple from each other, and the adsorption to each surface reduces to the single surface behavior.

As in the single surface case, it is advantageous to separate the different length scales. First, we compare the single surface adsorption length  $D_1$ , with the inter–surface separation w. At large separations  $w/2 \gg D_1$  the surfaces interact weakly and the polyelectrolytes recover the single surface profiles. On the other hand, at short inter–surface distances  $w/2 \ll D_1$ , the gap is too small for the polyelectrolytes to follow the single surface profile. In this limit the relevant length scale (eq. 18) is just D = w/2, since w/2 serves as a lower cutoff for D. When w/2 increases so that  $w/2 \simeq D_1$ , the profile becomes more complex and our main assumption is no longer valid. Nevertheless, as demonstrated below this simplified picture reproduces the main features that characterize the inter–surface interactions in those short distances,  $w/2 \leq D_1$ .

Furthermore, the effect of screening can be taken into account by separating the screening length from the two other length scales. Two opposite limits are considered (i) The low salt regime  $\kappa_s^{-1} \gg D_1$  and (ii) The high salt regime  $\kappa_s^{-1} \ll D_1$ .

A. Low Salt Regime: 
$$\kappa_s^{-1} \gg D_1$$

In the low salt regime the screening length is much larger than the width of the adsorbed layer and the effect of the small ions on the structure of the adsorbed layer can be neglected. This assumption amounts to neglecting the entropic contribution to the free energy  $f_{\text{ions}}(\mathbf{r})$  (eq. 3) and the electrostatic energies of the small ions in  $f_{\text{el}}(\mathbf{r})$  (eq. 4).

1. Large Distances: 
$$w/2 \gg D_1$$

At large distances  $w/2 \gg D_1$ , the two surfaces are only weakly coupled. The structure of the adsorbed layer near each of the two surfaces reduces to the single surface profile, and the "decorated" surfaces interact through a weak double layer interaction. In the limit of large distances and low salt conditions one needs to address the question of the relative size of w/2 and  $\kappa_s^{-1}$  as both lengths are large.

The free energy of an isolated adsorbing surface can be approximated by [26]

$$\beta F_p^{(1)}(C,D) = \alpha_1 \frac{a^2}{6D} C - \alpha_2 p |y_s| CD + 4\pi \beta_1 l_B p^2 C^2 D^3 + \frac{1}{2} \beta_2 v C^2 D \tag{19}$$

The first term is the polymer elastic energy (or connectivity) term, the second term is the electrostatic interaction of the monomers with the surface, and the third term is the Coulomb repulsion between the adsorbed monomers. The electrostatic terms can be derived by integrating the interaction of every pair of charged layers at distances x and x' from the surface, with charge densities (per unit area)  $d\sigma = pe\phi^2(x)dx$  and  $d\sigma' = pe\phi^2(x')dx'$ , respectively. Finally, the last term is the excluded volume term and will be neglected here since at low salt concentration its contribution is important only for extremely weakly charged polyelectrolytes.

The coefficients  $\alpha_1, \alpha_2, \beta_1$  and  $\beta_2$  are numerical prefactors, which depend on the exact shape of the dimensionless scaling function h(z). These coefficients can be explicitly calculated for a specific profile by integrating the Poisson

equation without taking into account the small ion contributions. For the simplest monotonous profile, namely a linear profile  $h_1(z)=z$  for  $0 \le z \le 1$  and  $h_1(z)=0$  for z>1, we get  $\alpha_1=1,\alpha_2=1/3,\beta_1=1/14$  and  $\beta_2=1/5$ . For a non-monotonous parabolic profile,  $h_2(z)=4z(1-z)$  for  $0 \le z \le 1$  and  $h_2(z)=0$  elsewhere, we get  $\alpha_1=16/3,\alpha_2=8/15,\beta_1\simeq 1/9$  and  $\beta_2\simeq 2/5$ . Another profile which we consider is an intermediate profile of the form  $h_3(z;\eta)=4/\eta^2z(\eta-z)$  for  $0 \le z \le 1$  and  $h_3(z)=0$  elsewhere, where  $\eta$  is a parameter. This profile is non-monotonous and has a finite value at z=1, which corresponds to the symmetry plane between the two surfaces. Furthermore, the special cases  $\eta \gg 1$  and  $\eta=1$  reduce to the simple linear and parabolic profiles  $h_1(z)$  and  $h_2(z)$ , respectively. The parabolic profile  $h_2(z)$  is a good choice for an isolated adsorbing surface in contact with a bulk of low concentration, whereas  $h_1(z)$  describes better interacting surfaces at small separation. The third profile  $h_3(z;\eta)$  can be regarded as intermediate between the other two. We stress that our scaling results do not depend on the specific shape of the profile h(z). Only the numerical prefactors will change.

The single surface free energy (eq. 19) can be minimized with respect to both D and C along the same lines as was done in ref. [26]. This yields a length scale  $D_1$  characterizing the adsorption onto a single surface

$$D_1 \simeq \frac{a}{p^{1/2}|y_s|^{1/2}} \tag{20}$$

and a concentration scale

$$C_1 \simeq \frac{|y_s|^2}{l_B a^2} \tag{21}$$

In the low salt limit screening effects can be neglected as long as the screening length  $\kappa_s^{-1}$  is much larger than the adsorption length  $D_1$ . This condition limits the low salt regime to

$$c_b \ll \frac{p|y_s|}{l_B a^2} \tag{22}$$

Inserting the above expressions back in the free energy gives the single surface free energy (up to numerical factors):

$$\beta F_p^{(1)} \simeq -\frac{p^{1/2}|y_s|^{5/2}}{l_b a} \tag{23}$$

At distances larger than the adsorbed layer  $x > D_1$  the amount of polyelectrolytes is small and comparable to its (low) bulk value. Since  $p\phi_b^2 \ll c_b$  (even in the low salt limit), the interaction at large distances can be simplified. The system can be regarded as a solution containing electrolytes only (no polyelectrolytes) between two effective surfaces positioned at the edge of the adsorbed layers  $x = \pm (w/2 - D_1)$ . The effective inter–surface distance is now  $w_{\text{eff}} = w - 2D_1$  and each surface is kept at a (reduced) potential  $y_D = \beta e \psi_D$  which is much smaller in magnitude than the original surface potential  $|\psi_D| \ll |\psi_s|$ .

In the absence of polyelectrolytes in the effective gap, the electrostatic potential between to charged surfaces can be obtained by solving the Poisson–Boltzmann equation [30]:

$$\nabla^2 \psi(\mathbf{r}) = \frac{8\pi e}{\varepsilon} c_b \sinh(\beta e \psi) \tag{24}$$

The above equation can be obtained from eq. 5 in the no polyelectrolyte limit. After the differential equation has been solved with the appropriate boundary conditions (namely,  $\psi = \psi_D$ ), the repulsive free energies and inter–surface

forces can be calculated. In particular, eq. 24 can be solved analytically in the weakly coupled regime,  $\kappa_s^{-1} \ll w_{\rm eff}/2$ , yielding the following expressions for the repulsive inter–surface interactions:

$$\beta \Delta F_{\text{el}} = 64c_b \kappa_s^{-1} \tanh^2(y_D/4) e^{-\kappa_s w_{\text{eff}}} \simeq 16c_b \kappa_s^{-1} y_D^2 e^{-\kappa_s w_{\text{eff}}}$$
(25)

$$\beta \Pi_{\rm el} = 64c_b \tanh^2(y_D/4) e^{-\kappa_s w_{\rm eff}} \simeq 16c_b y_D^2 e^{-\kappa_s w_{\rm eff}}$$
(26)

Other electrostatic regimes exist in which eq. 24 can be solved analytically. Those regimes lie beyond the scope of the present study because the polymer adsorbed layer reduces substantially the electric potential. Unfortunately, our model is too simple to give an accurate estimate of  $y_D$  which is a local property. For this purpose more refined models are required.

2. Short Distances; 
$$w/2 \ll D_1 \ll \kappa_s^{-1}$$

At short separations  $w/2 \ll D_1 \ll \kappa_s^{-1}$  the relevant length scale in eq. 18 is w/2 instead of D. Consequently, and due to the planar symmetry of the system, the polymer contribution to the free energy can be written as  $F_p(C, w) = 2F_p^{(1)}(C, D = w/2)$  where  $F_p^{(1)}(C, D)$  is the single surface free energy (eq. 19).

The free energy is minimized now only with respect to C leading to

$$C \simeq \frac{|y_s|}{l_B p} \frac{w^2 - w_{\min}^2}{w^4} \tag{27}$$

where  $w_{\min}^2 = 2\alpha_1 a^2/3\alpha_2 p|y_s|$ . The condition that C be positive, limits the validity of eq. 27 to distances larger than a minimal distance  $w_{\min}$ , while at shorter distances C = 0 and the polymers are depleted from the region between the surfaces. We estimate  $w_{\min} \simeq 0.2D_1$  and so eq. 27 is valid in the range  $0.1D_1 < w/2 < D_1$  [36].

The total amount of monomers (per unit area) adsorbed between the two surfaces is directly related to C and  $C_1$ :

$$\Gamma(w) = \int_{-w/2}^{w/2} \phi^2(x) dx = \begin{cases} 0 & w < w_{\min} \\ \alpha_2 w C(w) & w_{\min} < w < 2D_1 \\ 2\alpha_2 D_1 C_1 & 2D_1 < w \end{cases}$$
(28)

Similarly, the average reduced monomer concentration is given by

$$\left\langle \frac{\phi^2}{\phi_b^2} \right\rangle = \frac{\Gamma(w)}{w\phi_b^2} = \begin{cases}
0 & w < w_{\min} \\
\alpha_2 C(w)/\phi_b^2 & w_{\min} < w < 2D_1 \\
2\alpha_2 D_1 C_1/w\phi_b^2 & 2D_1 < w
\end{cases} \tag{29}$$

The adsorption properties  $\Gamma(w)$  and  $\langle \phi^2/\phi_b^2 \rangle$  are plotted in Fig. 12 as function of the inter–surface distance w for the same physical values of Fig. 4. Our results agree qualitatively with the numerical results of Fig. 4 and reproduce the three different adsorption regimes.

Inserting the above expression for C (eq. 27) back into the free energy, yields:

$$\beta F_p \simeq -\frac{|y_s|^2}{l_B} \frac{(w^2 - w_{\min}^2)^2}{w^5} \tag{30}$$

for  $w_{\min} < w < 2D_1$ . At distances shorter than  $w_{\min}$ , the polyelectrolyte is depleted from the gap, and the intersurface interaction is dominated by electrostatic repulsion [35].

The inter-surface force  $\Pi_p$  is readily obtained by differentiating the free energy  $F_p$  with respect to w

$$\beta \Pi_p = -\frac{\delta(\beta F_p)}{\delta w} \simeq -\frac{|y_s|^2}{l_B} \frac{(w^2 - w_{\min}^2)(w^2 - 5w_{\min}^2)}{w^6}$$
(31)

A quantitative comparison with the numerical results is shown in Fig. 13 where the physical parameters are the same as in Fig. 6. In Fig. 13 the polymer contribution to the excess free energy  $\Delta F_p(w) = F_p(w) - 2F_p^{(1)}$  and to the inter–surface force  $\Pi_p$  are plotted as functions of the inter–surface separation w. The single surface free energy  $F_p^{(1)}$  is calculated from eq. 23. Only small separations  $w < 2D_1$  are shown in the figure. For  $w > 2D_1$  the shape of the inter-surface profile is more complex and we do not have scaling arguments relating the polymer profiles with the force. However, we expect the polymer contribution to be small. Comparing Figs. 13 with 6, we note that our scaling results (the characteristic length scale as well as the characteristic force) are in good agreement with the numerical results for several p values.

B. High Salt Regime: 
$$\kappa_s^{-1} \ll D_1$$

In the high salt regime the screening length is much smaller than the adsorption length  $D_1$ . The Coulomb interactions between the charged monomers and the surface and between the monomers themselves decay exponentially with the Debye-Hückel screening length  $\kappa_s^{-1}$ .

Our calculation is based on estimating the polymer contribution to the forces as mediated by the small ions. One should bear in mind that the contribution of the small ions to the forces is no longer negligible and can explain the discrepancy between the numerical (exact) and the scaling results. It is hard to get an analytical estimate to the small ions contribution because their concentration depends on the polymer profile via the electric potential.

1. Large Distance: 
$$w/2 \gg D_1$$

The free energy (eq. 19) can be generalized by introducing  $\kappa_s^{-1}$  as a cut-off on the range of the electrostatic interactions (similar to what was done in Ref. [26] for the single surface case):

$$\beta F_p(C, D) = \alpha_1 \frac{a^2}{6D} C - \alpha_2 p |y_s| C \kappa_s^{-1} + 4\pi \beta_1 l_B p^2 \kappa_s^{-2} C^2 D + \frac{1}{2} \beta_2 v C^2 D$$
(32)

The electrostatic cut-off appears in two places. In the second term, only the first layers up to a distance  $\kappa_s^{-1}$  from the surface interact with the surface charges. In the third term, each layer interacts only with its neighboring layers in the range of  $\kappa_s^{-1}$ . The numerical values of the prefactors  $\alpha_1, \alpha_2, \beta_1$  and  $\beta_2$  can in principle be different from the low salt values. However, since the prefactors are only used in Fig. 14 to demonstrate the qualitative behavior we will arbitrarily set their values to be the same as in the low salt regime.

Minimizing eq. 32 with respect to D and C yields

$$D_1 \simeq \frac{\kappa_s a^2}{p|y_s|} \sim \frac{c_b^{1/2}}{p} \tag{33}$$

and

$$C_1 \simeq \frac{p^2 |y_s|^2 / (\kappa_s a)^2}{\beta_1 p^2 / c_b + \beta_2 v} \tag{34}$$

which are now also functions of the salt concentration  $c_b$  and  $\kappa_s = (8\pi l_B c_b)^{1/2}$ . The condition that the screening length is much smaller than the adsorption length amounts to

$$c_b \gg \frac{p|y_s|}{8\pi l_B a^2} \tag{35}$$

in agreement with the boundary of the low salt regime (eq. 35).

The single surface free energy is now:

$$\beta F_p^{(1)} \simeq -\frac{p^3 |y_s|^3 \kappa_s^{-3}}{(\beta_1 p^2 / c_b + \beta_2 v) a^2} \tag{36}$$

As in the low salt regime, the two adsorbed layers interact electrostatically. However, since the screening length is much shorter than the adsorption length in the high salt regime, this interaction decays quite rapidly. We note that the high salt regime can be further divided into two sub-regimes depending on the ratio of the two terms in the denominator of  $C_1$  and  $F_p^{(1)}$  as was discussed in Ref. [26].

2. Short Distances:  $w/2 \ll D_1$ 

At short distances, the relevant length scale in the free energy eq. 32 is w/2 instead of D (as in the low salt regime). The free energy can be minimized with respect to C yielding

$$C \simeq \frac{p|y_s|\kappa_s^{-1}}{\beta_1 p^2 / c_b + \beta_2 v} \frac{w - w_{\min}}{w^2}$$
 (37)

where  $w_{\min} = \alpha_1 \kappa_s a^2/3\alpha_2 p|y_s|$ . As in the low salt case, C is positive only for  $w > w_{\min} \simeq 0.2D_1$ . At smaller separations the polyelectrolytes are depleted from the gap and the inter-surface interaction is dominated by the electrostatic repulsion. We also note that the validity of eq. 32 requires that  $w \gg 2\kappa_s^{-1}$ .

The polymer free energy of interaction is now

$$\beta F_p \simeq -\frac{p^2 |y_s|^2 \kappa_s^{-2}}{\beta_1 p^2 / c_b + \beta_2 v} \frac{(w - w_{\min})^2}{w^3}$$
(38)

and the inter-surface force

$$\beta \Pi_p \simeq -\frac{p^2 |y_s|^2 \kappa_s^{-2}}{\beta_1 p^2 / c_b + \beta_2 v} \frac{(w - w_{\min})(w - 3w_{\min})}{w^4}$$
(39)

The qualitative behavior described by eqs. 38 and 39 is similar to that of the low salt regime (eqs. 30, 31). The typical behavior for a strong polyelectrolyte is depicted in Fig. 14, where the same physical parameters of Fig. 10 are used. We note that the quantitative agreement between the numerical (Fig. 10) and scaling (Fig. 14) results is not as good as in the low salt limit. For example, the value of the minimum in the free energy is about three times smaller in Fig. 14 as compared with Fig. 10. Also the variation of w at this minimum with the salt concentration is weaker in the numerical results. As discussed above, the main source of discrepancy between the numerical and scaling results is the omission of the small ion contribution in the latter.

#### C. Discussion

To summarize our results we present in Fig. 15, a schematic diagram of the different adsorption regimes. The dashed lines mark the single surface adsorption regimes in terms of the charge fraction p and the salt concentration  $c_b$ . Three adsorption regimes can be distinguished:

- The low salt regime  $c_b \ll p|y_s|/8\pi l_B a^2$ .
- The first high salt (HS I) regime  $c_b \gg p|y_s|/8\pi l_B a^2$  with weak polyelectrolytes  $p^2 \ll v c_b$ .
- The second high salt (HS II) regime  $c_b \gg p|y_s|/8\pi l_B a^2$  with strong polyelectrolytes  $p^2 \gg v c_b$ .

The shaded area in Fig. 15 marks the region in parameter space where the polymer contribution to the inter–surface interaction is comparable to or larger than the pure electrostatic contribution. The shaded area includes the low salt regime, a large portion of the HS II (high salt/strong polyelectrolyte) regime and a small portion of the HS I (high salt/weak polyelectrolyte) regime. The exact crossover lines depend, of course, on the numerical coefficients which are not included in our approximations. Nevertheless, the qualitative picture can be deduced from the diagram. The different behaviors (as depicted previously) can be demonstrated with the help of this diagram. The filled circles in the low salt regime mark the graphs of Fig. 6 and are well within the shaded area. The filled squares on the right border of the diagram (at p = 1) correspond to the graphs of Fig. 10 representing strong polyelectrolytes in the high salt regime. At higher salt concentration the system is closer to the boundary of the shaded area and the polymer attraction is weaker. Finally, when the ionic strength is high enough the attractive contribution is too weak to be observed. Weak polyelectrolytes in the high salt regime belong to the top left side of the diagram outside of the shaded area. In this regime, the electrolyte dominates the inter–surface interactions which are purely repulsive, as is indeed the case for the force curves of Fig. 11. These curves are represented in Fig. 15 by filled triangles.

In the following, we briefly summarize our findings in the different adsorption regimes. In Sec. VI the findings are compared with experimental works which are reported in the literature.

Low Salt Regime: In the low salt regime, the Debye–Hückel screening length is much larger than the width of the adsorbed layer. As a result the electrostatic interactions of the charged monomers with the surfaces and their interactions with other monomers are unscreened. This leads to strong adsorption as can be seen from the numerical results shown in Figs. 3–4 and from the scaling results (eqs. 28, 29) shown in Fig. 12. In addition, since the bulk concentration of the salt and counter-ions,  $c_b$  and  $p\phi_b^2$  respectively, is small, the charge density in the solution between the two surfaces is mainly due to the charged monomers. This is demonstrated in Fig. 5, where it is shown that the surface charges are balanced by the charged monomers.

At large distances the adsorbed polymer forms two distinct layers on the two surfaces. The amount of polymer adsorbed between the two surfaces saturates to a constant value (Fig. 4) which is approximately twice the single surface adsorbed amount. As discussed in a preceding work [26], the width of the single surface adsorbed layer  $D_1$  and the single surface adsorbed amount  $\Gamma_1$  both scale as  $p^{-1/2}$ . The dependence on p is due to the balance between the attraction of the monomers to the surface which is proportional to p and the monomer—monomer Coulomb repulsion

which is proportional to  $p^2$ . The fact that the adsorbed amount decreases when the polymer charge increases reflects the energy barrier for bringing a large amount of charged monomers to the vicinity of the charged surface.

The two layers start to overlap when the inter-surface distance is about twice the width of the single surface adsorbed layer  $w \simeq 2D_1$ . Below this distance the adsorbed amount slightly increases (Fig. 4) and the two surfaces strongly attract each other (Fig. 6). Our scaling approach recovers the increase in the adsorbed amount (eq. 28 and Fig. 12) and the attraction of the two surfaces (eqs. 30,31 and Fig. 13). The magnitude of the polymer contribution to the interaction free energy scales as

$$\beta \Delta F_p \sim \frac{p^{1/2} |y_s|^{1/2}}{l_{Ba}}$$
 (40)

This energy scale should be compared with the electrostatic interaction energy which scales as

$$\beta \Delta F_{el} \sim c_b \kappa_s^{-1} |y_s|^2 \tag{41}$$

The condition that  $\Delta F_p$  will be at least comparable to  $\Delta F_{el}$  limits the salt concentration to

$$c_b < \frac{p|y_s|}{l_B a^2} \tag{42}$$

in agreement with the boundary of the low salt regime (eq. 22).

If the inter–surface distance is further reduced, the entropy loss due to the confinement of the polymer to a narrow slit pushes the polymer out of the gap between the two surfaces. This can be seen from the numerical results (Fig. 4) and also from eq. 27, where  $w_{\min}$  is the minimal distance below which the polymer is compelled to leave the gap.

High Salt Regime: In the high salt regime the Debye–Hückel screening length  $\kappa_s^{-1}$  is much smaller than the width of the adsorbed layer. As a result the range of the electrostatic interactions is much shorter and each charged monomers interacts only with monomers at a distance smaller than  $\kappa_s^{-1}$ .

The limiting behavior at large distances depends strongly on the charge fraction p. For weak polyelectrolytes where p is small (regime HS I) the monomer–monomer Coulomb repulsion which is proportional to  $p^2$  is negligible and the single surface adsorbed amount  $\Gamma_1$  scales as  $p/c_b^{1/2}$ . On the other hand, for strong polyelectrolytes where p is large (regime HS II) the monomer–monomer Coulomb repulsion is dominant and the single surface adsorbed amount  $\Gamma_1$  scales as  $c_b^{1/2}/p$ . The latter behavior is similar to that of the low salt regime with a different p dependence. At higher salt concentration the adsorbed amount increases as the monomer–monomer Coulomb repulsion at the adsorbed layer is screened out.

In the high salt case, the contribution of the small ions to the charge density can not be neglected. As seen in Fig. 9, about two thirds of the surface charge are balanced by small ions and only one third by charged monomers. Another interesting aspect of the interplay between charged polymer chains and small ions is the spatial distribution of charges between the two surfaces. The polyelectrolytes are strongly adsorbed on the surface resulting in a sign reversal of the potential: it is negative at the surface and becomes positive at a distance of 6-7Å. In order that the system will be overall neutral the central region between the two surfaces has an excess of negative ions as seen in Fig. 8. At short distances (less than 12-14Å) this effect disappears and the potential is negative everywhere in the gap. As seen from Fig. 10 and eq. 17 the sign reversal of the mid-plane potential y(x=0) is accompanied by a sign

reversal in the inter–surface force  $\Pi(w)$ . The potential sign reversal can also be seen in the low salt regime. Since the concentration of small ions is very small, the over-compensation effect is weak.

When the two surfaces are brought closer together,  $w < 2D_1$ , these layers start to overlap (See Fig. 7) and the adsorbed amount slightly increases. At this separation, strong polyelectrolytes induce strong attraction between the two surfaces (Fig. 10). The polymer contribution to the attraction can be estimated from our scaling approach to be

$$\beta \Delta F_p \sim \frac{p^3 |y_s|^3 \kappa_s^{-3}}{(\beta_1 p^2 / c_b + \beta_2 v) a^2} \tag{43}$$

Following the low-salt discussion we compare this interaction with the electrostatic interaction energy (eq. 41). For weak polyelectrolytes  $p^2 \ll vc_b$  (regime HS I) the polymer contribution dominates for

$$c_b^2 < \frac{p^3|y_s|}{l_B a^2 v} \tag{44}$$

while for strong polyelectrolytes  $p^2 \gg vc_b$  the polymer contribution is dominant at low salt concentration

$$c_b \ll \frac{p|y_s|}{l_B a^2} \tag{45}$$

At very short distances  $w < w_{\min}$  (eq. 37), the polymer is depleted from within the gap as can be also seen in Fig. 9.

#### V. IRREVERSIBLE ADSORPTION

So far in this study we have assumed that the adsorbed layer is in thermodynamic equilibrium with a bulk reservoir. Hence the total amount of adsorbed monomers can vary and is determined by the free energy minimization (eqs. 1-4). However, in physical systems the energetic barrier for detaching an adsorbed chain from the surface can be much larger than the thermal energy  $k_BT$ . As a result the relaxation times towards equilibrium can be much larger than the experimental time scales. In this case, one can consider the amount of adsorbed monomers as fixed.

In this section we study the effect of irreversible adsorption by excluding the possibility of polymer exchange with the reservoir while keeping the total amount of monomers adsorbed between the two surfaces fixed. For simplicity we limit ourselves to the low–salt case. The results can be generalized to the high salt case. In principle, the state of the system is determined by minimizing the free energy (eqs. 1-4) under the constraint that

$$\int_{-w/2}^{w/2} \phi^2(x) dx = \Gamma_0 \tag{46}$$

where  $\Gamma_0$  is the predetermined value of the amount of polymer between the surfaces. This constraint can be introduced through a Lagrange multiplier  $\lambda$  replacing the chemical potential term in F so that the functional to be minimized becomes

$$\beta \tilde{F} = \beta F - \lambda \left( \int_{-w/2}^{w/2} \phi^2(x) dx - \Gamma_0 \right)$$
 (47)

The self–consistent field equation now reads

$$\frac{a^2}{6}\nabla^2\phi(\mathbf{r}) = v\phi^3 + p\phi\beta e\psi - \lambda\phi \tag{48}$$

while the modified Poisson–Boltzmann equation (eq. 5) is not affected by the irreversibility of the adsorption process, because the counter-ions are still free to exchange between the reservoir and the adsorbed layer.

Equations 5 and 48 are solved under the constraint of eq. 46 where  $\lambda$  is adjusted to give the desired value of  $\Gamma_0$ . Typical force profiles calculated numerically are presented in Fig. 16a, where the free energy  $2\pi\Delta F$  is plotted as a function of the inter–surface distance w. For comparison we plot on the same graph the equilibrium free energy (solid curve) of Fig. 6. The dotted curve was calculated for the same physical values with the additional constraint that the total amount of monomers adsorbed between the surfaces is fixed to the equilibrium value of single surface adsorption (or equivalently two surfaces held at large distances). This value is defined as  $\Gamma_{\rm sat}$ . As can be seen from Fig. 4a for p=1,  $\Gamma_{\rm sat}=0.011 {\rm \AA}^{-2}$ .

The free energy difference between the solid and dotted curves is quite small and appears only at short distances when the adsorbed amount in true equilibrium starts to deviate from its saturated value (see also Fig. 4). Different values of  $\Gamma_0$  are shown on Fig. 16a. For low values of  $\Gamma_0$  (e.g.  $\Gamma_0 = \Gamma_{\rm sat}/2$ ) the attraction is weaker, while for higher values (e.g.  $\Gamma_0 = 2\Gamma_{\rm sat}$ ) the attraction is much stronger.

In order to understand better this behavior we return to the scaling approximation where we consider first the case of irreversible adsorption on a *single* surface. We assume that a fixed amount  $\Gamma = \Gamma_0/2$  is adsorbed to the surface. Since the adsorbed amount  $\Gamma$  is related to the length scale D and the concentration scale C through  $\Gamma = \alpha_2 CD$ , it is possible to express C in terms of D and thus the free energy (eq. 19) in terms of D and  $\Gamma_0$ . Neglecting the excluded volume term, equation 19 now becomes:

$$\beta F_p^{(1)}(\Gamma_0, D) = \frac{\alpha_1}{12\alpha_2} \frac{a^2}{D^2} \Gamma_0 - \frac{1}{2} p |y_s| \Gamma_0 + \frac{\pi \beta_1}{\alpha_2^2} l_B p^2 \Gamma_0^2 D \tag{49}$$

Minimization of the free energy with respect to D yields

$$D_{\rm irr} \simeq \left(\frac{a^2}{l_B p^2 \Gamma_0}\right)^{1/3} \tag{50}$$

Substituting  $D_{\rm irr}$  back in the free energy gives

$$\beta F_p^{(1)} \simeq -\frac{1}{2}p|y_s|\Gamma_0 + a^{2/3}l_B^{2/3}p^{4/3}\Gamma_0^{5/3}$$
(51)

where we have omitted some numerical coefficients. The first term in eq. 51 is simply the interaction energy of the charged monomers with the surface while the second term is a balance between the monomer–monomer Coulomb repulsion and the chain elasticity term.

When the two surfaces are interacting with each other, we can write an explicit expression for  $F_p(w)$  at small distances ( $w \ll D_{\rm ir}$ ) by replacing the adsorption length scale D with w/2. The free energy then becomes:

$$\beta F_p(w) = \frac{2\alpha_1}{3\alpha_2} \frac{a^2}{w^2} \Gamma_0 - p|y_s|\Gamma_0 + \frac{\pi\beta_1}{\alpha_2^2} l_B p^2 \Gamma_0^2 w$$

$$\tag{52}$$

The interaction free energy is now  $\Delta F_p = F_p(w) - 2F_p^{(1)}$ . The surface interaction term cancels out and we are left with three terms: two positive terms from eq. 52 and a negative term from eq. 51. The latter scales as  $\Gamma_0^{5/3}$  and is responsible to the attraction at short distances where the third term of eq. 52 becomes small. In Fig. 16b we plot the interaction free energy as calculated from eqs. 51,52 for the same physical values as in Fig. 16a. Although the

numerical coefficients can not be obtained accurately from this approach the qualitative behavior is in accord with the numerical results.

### VI. COMPARISON WITH EXPERIMENTS

The experimental studies with the Surface Force Apparatus [5–12] focus mostly on the repulsive interactions between adsorbing surfaces. Due to the limitations of the experimental technique, the attractive interactions at short distances appear as jumps in force–distance profiles. Nevertheless, some of the qualitative features can be deduced from the experiments and agree with our findings.

Luckham and Klein [5] have measured interactions between mica surfaces in the presence of poly-L-lysine which is a strong polyelectrolyte (p=1) at two different salt concentrations  $c_b = 1$ mM and  $c_b = 0.1$ M. The inter-surface forces  $\Pi_R(w)$  (eq. 15) were measured at distances  $50\text{\AA} < w < 1200\text{\AA}$ . The forces were always repulsive, decaying exponentially as function of w with decay lengths comparable to the Debye-Hückel screening length  $\kappa_s^{-1}$ . These forces can be interpreted as the electrostatic repulsion between two adsorbed layers at distances larger than the width of a single layer (eq. 25). Significant deviations were found between the first approach where the two surfaces are brought close together and subsequent decompression-compressions cycles. The amplitude of the repulsion in the latter case was strongly reduced while the decay length of the force remained quite the same. In addition, the amount of polymer adsorbed between the two surfaces, as estimated by refractive index measurements, was much higher than in the initial measurements. Those effects demonstrate that the adsorbed layers are not always in equilibrium and that compression might lead to strong adsorption of charged polymers. The adsorbed amount remains high when the surfaces are separated from each other due to the high energetic barrier for desorption. The reduction in the inter-surface repulsion when the adsorbed amount is high is in accord with our numerical and analytical results for the case of irreversible adsorption (Sec. V).

Marra and Hair [6] have adsorbed poly(2-vinylpyradine) (P2VP) between mica surfaces. The pH of the solution was such that the polymer was fully charged (p = 1) during the experiments. At low salt concentrations the forces were repulsive at large distances with an exponential decay which is consistent with the Debye–Hückel screening length. Attraction of about -7mN/m was detected at distances between 11 and 40Å. In the presence of 0.01M NaCl the magnitude of the repulsive forces increased while the attraction was reduced to -3mN/m and shifted to distances between 25 and 80Å. At even higher ionic strengths (0.1M NaCl) the attraction disappeared altogether but an additional non–exponential contribution to the inter–surface repulsion was detected at distances between 60 to 100Å. These results confirm our findings that the effect of salt is to increase the adsorption length  $D_1$  and to reduce the polymer attractive contribution to the inter–surface interactions.

Claesson and Ninham [7] have adsorbed chitosan, a cationic biopolymer of glucosamine segments, between mica surfaces in the presence of 0.01 wt % acetic acid. The chitosan charge fraction was controlled through the pH of the solution

$$p = \frac{10^{-(pH-pK_0)}}{1+10^{-(pH-pK_0)}}$$
(53)

where  $K_0 = 10^{-pK_0} \simeq 10^{-6.5}$  is the dissociation constant of the chitosan monomers. At low pH, the polymer is fully charged and the interactions were repulsive in the first compression when the surfaces were brought into contact. A double layer repulsion was detected at large distances (w > 100Å) and strong steric repulsion at shorter distances. Upon separation, attraction was detected at distances around 20 - 25Å. At pH=6.2 ( $p \simeq 2/3$ ) the repulsive double layer interaction disappeared altogether. The disappearance of the electrostatic double layer interaction indicates that the surface charges are exactly balanced by the adsorbed polymers. Attraction was detected at distances of about 20 - 25Å and strong steric repulsion at shorter separations. At pH=9.1 where the polymer was only weakly charged ( $p \simeq 1/400$ ) the double layer repulsion was again the dominant interaction.

Dahlgren et al. [8] have studied the effect of salt concentration by adsorbing poly ((3-methacrylamido propyl) -trimethyl-ammonium chloride) (MATPAC) between mica surfaces. Three salt concentrations were considered  $c_b = 0.1 \text{mM}$ , 0.01M and 0.1M. The forces were repulsive at large distances and decayed exponentially with decay lengths of 170Å, 30Å and 11Å, respectively. The first decay length is smaller than the Debye–Hückel screening length of the corresponding salt concentration ( $\kappa_s^{-1} \simeq 300\text{Å}$ ) due to the contribution of the counter-ions. At higher salt concentrations this contribution is negligible and the decay lengths agree with the expected screening lengths. Attractive interactions were detected at short distances of a few nanometers. The magnitude of these attractive forces decreased as the amount of salt increased in agreement with the numerical results of Fig. 10.

In another work, **Dahlgren et al.** [9] have studied the effect of both charge fraction and salt concentration on the inter–surface forces. Three different polyelectrolytes with different charge fractions p were used: MAPTAC (p=1) and two copolymers AM-CMA-10 (p=0.1) and AM-CMA-30 (p=0.3) which were prepared using different ratios of neutral acrylamide (AM) segments and positively charged (2-acroyloxy ethyl) -trimethyl-ammonium chloride (CMA) segments. For a fixed charge fraction (p=0.3) three different ionic strengths were compared:  $c_b=0.1$ mM,  $c_b=0.0$ 1M and  $c_b=0.1$ M. These experiments correspond to a vertical scan in Fig. 15. At the lowest ionic strength, the system is in the low salt regime and strong attraction is detected at intermediate distances 40 < w < 100Å. At the next ionic strength ( $c_b=0.0$ 1M) the system is in the lower part of the high salt regime and weak attraction is still observed at distances below 60Å. At the higher value of  $c_b=0.1$ M no attractive interactions are observed and the electrostatic repulsions dominate the inter–surface forces. For a fixed ionic strength ( $c_b=0.1$ mM) Dahlgren et al. have compared the inter–surface interactions for three different charge fractions: p=0.1, p=0.3 and p=1. This set of experiments corresponds to a horizontal cut in Fig. 15. At the lowest charge fraction the repulsive interactions are dominant while for higher values of p attractions is observed at distances below  $w \simeq 100$ Å.

Finally, the effect of ionic strength was studied separately by **Dahlgren** [11]. Two polyelectrolytes, poly (2-proplyionyloxy ethyl) -trimethyl-ammonium chloride) (PCMA) and MAPTAC which have different molecular weight but the same charge fraction (p=1) were studied. The monomers of these polymers are large and therefore the regime boundaries in Fig. 15 should be shifted to lower salt concentrations. Dahlgren has compared several types of multivalent salts at intermediate ionic strengths which are equivalent to  $c_b = 0.1, 0.2, 0.3$  and 0.6mM. In the higher ionic strengths (0.3 and 0.6mM) no attractive interactions were observed. However, at lower ionic strengths attraction was observed at distances below  $w \simeq 120\text{Å}$  and  $w \simeq 180\text{Å}$  for  $c_b = 0.1\text{mM}$  and  $c_b = 0.2\text{mM}$ , respectively. The ratio between the two lengths scales is approximately  $\sqrt{2} \simeq 1.4$  in agreement with the adsorption length scale in the high

salt regime  $D_1 \sim c_b^{1/2}$  (eq. 33). Furthermore, the adhesion force was measured as  $\Pi_{\rm ad} \simeq 170$  mN/m and  $\Pi_{\rm ad} \simeq 250$  mN/m in agreement with the force scale of strong polyelectrolytes in regime HS II  $F_p \sim 1/c_b^{1/2}$  (eq. 43).

### VII. CONCLUSIONS

In this paper we calculated numerically concentration profiles of polyelectrolytes between two charged surfaces and studied the inter–surface interactions as a function of the distance between the charged surfaces. Over–compensation of surface charges by adsorbed monomers was found to be strongly related to the reversal of inter–surface forces from repulsion to attraction at short distances where the two adsorbing layers strongly overlap.

The effect of the polymer charge and ionic strength on the inter–surface interaction is studied by means of a simple variational approach. Three main regimes are found: (i) a low salt regime,  $c_b \ll p|y_s|/8\pi l_B a^2$ ; (ii) a high salt regime  $c_b \gg p|y_s|/8\pi l_B a^2$  for weak polyelectrolytes  $p^2 \ll vc_b$  (HS I); and (iii) a second high salt regime for strong polyelectrolytes  $p^2 \gg vc_b$  (HS II).

In the low salt regime, strong repulsion at very short distances is a result of the polymer depletion from the intersurface gap. As the distance increases to  $w \sim a/p^{1/2}$ , strong attraction is due to overlap of the adsorbed layers. Finally, when the inter-surface separation is larger than twice the adsorption length of a single surface, the two adsorbed layers separate and repel each other electrostatically. In the HS II regime the behavior is similar to the low salt one, with a modified length scale of interaction given by  $\kappa_s a^2/p$ . On the other hand, in the HS I regime, the polyelectrolyte attractive contribution is too weak to generate a similar attraction at short distances. Consequently, the inter-surface interaction is repulsive with a decay length of  $\kappa_s^{-1}$ .

Some of the features described above are also present in the discrete lattice model of Böhmer et al. [18]. In particular, attractive interactions between equally charged surfaces were obtained numerically (Fig. 9 of Ref. [18]). This attraction was attributed to bridging by polymer chains from one surface to the other. The lattice model contains information regarding the fine details of the polymer chains which are absent in our model. On the other hand, the continuum approach is a convenient starting point for analytical approximations such as the scaling approach presented in this work. Attractive interactions were also obtained by Podgornik [27] for the case of fixed adsorbed amount and without considering the nonlinear excluded volume interaction. For polyelectrolytes in a poor solvent, Châtellier and Joanny [28] have obtained oscillations in the polymer concentration as well as in the inter–surface interactions.

The model presented here takes into account the important Coulombic degrees of freedom within the frame work of the Poisson-Boltzmann formalism. We solve the coupled non-linear equations for the electrostatic potential and polymer concentration which allows consistent treatment of excluded volume effects as well as strong potential and surface charges (not the linearized Debye-Hückel version). This allows us to consider cases where the Coulombic degrees of freedom are a major perturbation on the adsorption of neutral polymers.

In the same time our approach has several limitations, some of which can be improved. The polymers chains are treated within a mean-field approximation which misses certain properties of polymer statistics such as the chain connectivity, stiffening of the persistence length, finite chain corrections and more specific conformations of polymers close to surfaces (loops, tails and trains).

On the other hand, the simple model we present offers a qualitative picture of polyelectrolyte chains between surfaces and suggests several scaling regimes. It can be further improved to take into account more realistic situations such as surface heterogeneities and other geometries, various charge distributions (quenched and annealed) on the chains [24,25,37], pH effects for acidic and basic polyelectrolytes [26] as well as finite ion or monomer sizes [38–40].

In this work we have assumed constant surface potentials. One could also consider constant surface charges. In the low salt limit the behavior is expected to resemble the case of fixed amount of adsorbed polymer since the charged monomers are main source of charges which are able to neutralize the surface charges. In the presence of salt this is no longer the case and the behavior can differ considerable.

It would be interesting to have thorough experimental results on the effect of the charge fraction p and salt concentration  $c_b$  on the nature and magnitude of the forces and the corresponding length scales. We hope that our present work will encourage such systematic experimental studies.

# Acknowledgments

We would like to thank P. Claesson, H. Diamant, B. Jönsson, Y. Kantor, D. Langevin and S. Safran for useful discussions. Two of us (IB and DA) would like to thank the Service de Physique Théorique (CE-Saclay) and one of us (HO) the School of Physics and Astronomy (Tel Aviv University) for their warm hospitality. Partial support from the Israel Science Foundation founded by the Israel Academy of Sciences and Humanities – centers of Excellence Program and the U.S.-Israel Binational Foundation (B.S.F.) under grant No. 94-00291 gratefully acknowledged.

- [1] Joanny J. F., Leibler L. and de Gennes P. G., J. Pol. Sci. 1979, 17, 1073.
- [2] Cabane B., Wong K., Wang T. K., Lafuma F. and Duplessix R., Coll. Pol. Sci. 1988, 266, 101.
- [3] Dickinson E. and Eriksson L., Adv. Coll. Interface Sci. 1991, 34, 1, and references therein.
- [4] Israelachvili J. and Adams G. E., J. Chem. Soc. Faraday Trans. I 1978, 74, 975.
- [5] Luckham P. F. and Klein J., J. Chem. Soc. Faraday Trans. I 1984, 80, 865.
- [6] Marra J. and Hair M. L., J. Phys. Chem. 1988, 92, 6044.
- [7] Claesson P. M. and Ninham B. W., Langmuir 1992, 8, 1506.
- [8] Dahlgren M. A. G., Waltermo Å, Blomberg E., Claesson P. M., Sjöström L, Åkesson T. and Jönsson B., J. Phys. Chem. 1993, 97, 11769.
- [9] Dahlgren M. A. G., Claesson P. M. and Audebert R., Nord. Pulp. and Paper Research J. 1993, 8, 62.
- [10] Claesson P. M., Dahlgren M. A. G. and Eriksson L., Coll. Surf. A. 1994, 93, 293.
- [11] Dahlgren M. A. G., Langmuir 1994, 10, 1580.
- [12] Lowack K. and Helm C. A., Macromolecules 1998, 31, 823.
- [13] Bergeron V., Langevin D. and Asnacios A., Langmuir 1996, 12, 1550.
- [14] Van der Schee H. A. and Lyklema J., J. Phys. Chem. 1984, 88, 6661.
- [15] Papenhuijzen J., Van der Schee H. A. and Fleer G. J., J. Coll. Interface Sci. 1985, 104, 540.
- [16] Evers O. A., Fleer G. J. Scheutjens J. M. H. M. and Lyklema J., J. Coll. Interface Sci. 1985, 111, 446.
- [17] Van de Steeg H. G. M., Cohen Stuart M. A., de Keizer A. and Bijsterbosch B. H., Langmuir 1992, 8, 8.
- [18] Böhmer M. R., Evers O. A. and Scheutjens J. M. H. M., Macromolecules 1990 23, 2288.
- [19] Åkesson T., Woodward C. and Jönsson B., J. Chem. Phys. 1989, 91, 2461.
- [20] Granfeldt M.K., Jönsson B. and Woodward C. E., J. Phys. Chem. 1991, 95, 4819. Podgornik R., Åkesson T. and Jönsson B. J. Chem. Phys. 1995, 102, 9423.
- [21] Muthukumar M., J. Chem. Phys. 1987, 86, 7230.
- [22] Varoqui R., Johner A. and Elaissari A., J. Chem. Phys. 1991, 94, 6873.
- [23] Varoqui R., J. Phys. II (France) 1993, 3, 1097.

- [24] Borukhov I., Andelman D. and Orland H., Europhys. Lett. 1995, 32, 499.
- [25] Borukhov I., Andelman D. and Orland H., submitted to Eur. Phys. J. B
- [26] Borukhov I., Andelman D. and Orland H., Macromolecules, 1998, 31, 1665.
- [27] Podgornik R., J. Phys. Chem. 1992, 96, 695.
- [28] Châtellier X. and Joanny J. F., J. Phys. II (France) 1996, 6, 1669.
- [29] De Gennes P. G., Scaling Concepts in Polymer Physics; Cornell Univ.: Ithaca, 1979.
- [30] For a review see: Israelachvili J. N., Intermolecular and Surface Forces, 2nd ed.; Academic Press: London, 1990.
- [31] Recent measurements of inter–surface forces in the presence of asymmetric electrolytes (such as CaCl<sub>2</sub>) and without polyelectrolytes followed by theoretical calculations using the hyper-netted chain (HNC) scheme have indicated that ion correlations beyond mean field can lead to attraction of symmetric surfaces at very short separations of a few Angstroms, e.g., ref. [32].
- [32] Kjellander R., Marčelja S., Pashley R. M. and Quirk J. P., J. Chem. Phys. 1990, 92, 4399.
- [33] De Gennes P. G., Macromolecules 1981, 15, 1637.
- [34] De Gennes P. G., Macromolecules 1982, 15, 492.
- [35] Depletion forces contribute to inter–surface attraction. However this contribution is proportional to  $k_B T v \phi_b^4$  and is much smaller than the electrostatic repulsion.
- [36] Since the linear profile  $h_1(z)$  is a better approximation at small distances we use it in order to estimate the lower cutoff  $w_{\min}$ , while the coefficients of the parabolic profile  $h_2(z)$  is used in the calculation of the single surface adsorption length  $D_1$
- [37] Raphael E. and Joanny J. F., Europhys. Lett. 1990, 13, 623.
- [38] Eigen M. and Wicke E., J. Phys. Chem. 1954, 58, 702.
- [39] Kralj-Iglič V. and Iglič A., Electrotechnical Rev. (Slovenia) 1994, 61, 127. Kralj-Iglič V., Electrotechnical Rev. (Slovenia) 1995, 62, 104; Kralj-Iglič V. and Iglič A., J. Phys. II (France) 1996, 6, 477.
- [40] Borukhov I., Andelman D. and Orland H., Phys. Rev. Lett. 1997, 79, 435.

### FIGURE CAPTIONS

- Fig. 1: Schematic view of a polyelectrolyte solution between two parallel charged surfaces at a distance w from each other. The solution contains polyelectrolyte chains and small ions. The surfaces are kept at a constant potential.
- Fig. 2: (a) Two half cylinders with a  $90^{\circ}$  tilt between the axes, as used in the surface force apparatus to measure inter–surface forces. The radii R of the cylinders are of the order of 1-2 cm while w ranges down to a few Angstroms. (b) Two spheres of radii R at a distance w. Typically, colloidal suspensions contain particles whose radii are of a few microns down to hundreds of Angstroms, while the stability is determined by the balance of forces at much smaller distances.
- Fig. 3: Profiles of (a) the reduced electrostatic potential  $y = \beta e \psi$  and (b) the reduced monomer concentration  $\phi^2/\phi_b^2$  as functions of the position x between the two surfaces. The profiles were obtained by solving numerically the differential equations (eqs. 5,6) for several inter-surface distances. For comparison, the different profiles are plotted on the same axis so that all mid-planes (x=0) coincide. The surfaces are placed at different distances from the midplane as indicated by the filled squares. In the numerical examples in Figs. 3 to 11 we assume the following physical parameters: the polymer concentration is  $\phi_b^2 = 10^{-6} \text{Å}^{-3}$  with an effective monomer length a=5Å and excluded volume parameter  $v=50\text{Å}^3$ . It is immersed in an aqueous solution ( $\varepsilon=80$ ) at room temperature (T=300K) and the surfaces are kept at a constant potential  $y_s=\beta e\psi_s=-2$ . In addition, in the current figure the polymer charge fraction p=1 and the salt concentration  $c_b=1\text{mM}$ . The different curves correspond to separations of w=40Å (solid curve); w=20Å (dots); w=15Å (short dashes) and w=10Å (long dashes).
- Fig. 4: Adsorption of polyelectrolytes in a low salt solution between two charged surfaces for two different polymer charge fractions. (a) Total amount of monomers adsorbed between the surfaces per unit area Γ and (b) the average reduced monomer concentration  $\langle \phi^2/\phi_b^2 \rangle$  as functions of the inter–surface distance w. The salt concentration is  $c_b = 10^{-6}$ M. The different curves correspond to charge fractions of p = 1 (solid curve) and p = 0.2 (dashed curve).
- Fig. 5: Charge densities per unit area as function of the inter–surface distance w. The two positive (upper) curves correspond to the total amount of polymer charge adsorbed between the two surfaces per unit area  $\sigma_p = pe\Gamma$ . The two negative (lower) curves correspond to the induced surface charge density on both surfaces,  $2\sigma_s$ . The contribution of the small ions to the charge density is not displayed. The physical parameters and notations are the same as in Fig. 4.
- Fig. 6: Inter–surface interactions for polyelectrolytes between two surfaces held at a constant potential and in a low salt solution. (a) The excess free energy per unit area  $2\pi\Delta F$  as a function of the inter–surface distance w. The factor  $2\pi$  is used in order to enable direct comparison with SFA measurements (see eq. 15). (b) The force per unit area  $\Pi$  between the two surfaces as a function of the inter–surface distance w. The physical parameters and notations are the same as in Fig. 4.

- Fig. 7: Profiles of (a) the reduced electrostatic potential  $y = \beta e \psi$  and (b) the reduced monomer concentration  $\phi^2/\phi_b^2$  as function of the position x between the two surfaces. Same physical values and notations as in Fig. 3 except for a much higher value for the salt concentration,  $c_b = 1$ M. The different curves correspond to separations of w = 40Å (solid curve); w = 20Å (dots); w = 15Å (short dashes); w = 10Å (long dashes) and w = 7Å (dots and long dashes).
- Fig. 8: Profiles of the small ion concentration  $c^+$  and  $c^-$  as function of the position x between the two surfaces for two of the separations presented in Fig. 7: w = 40Å (solid curve) and = 10Å (long dashes).
- Fig. 9: Different contributions to the total charge density per unit area as function of the inter-surface distance w for highly charged polyelectrolytes (p=1) in the high salt limit  $(c_b=1\mathrm{M})$ . The different curves correspond to twice the induced surface charge density  $2\sigma_s$ , the total amount of polymer charge adsorbed between the two surfaces per unit area  $\sigma_p$ , and the total amount of charge carried by small ions  $(\sigma^+ + \sigma^-)$ .
- Fig. 10: Inter-surface interactions for highly charged polyelectrolytes (p=1) at high salt concentration. (a) The excess free energy per unit area  $2\pi\Delta F$  and (b) the force per unit area  $\Pi$  between the two surfaces as function of the inter-surface distance w. The salt concentration is  $c_b = 0.1 \mathrm{M}$  (solid curve) and  $c_b = 1 \mathrm{M}$  (dashed curve). The inset shows the mid-plane values of the reduced electrostatic potential y(0) as a function of w.
- Fig. 11: Inter-surface interactions for weakly charged polyelectrolytes (p = 0.1) at high salt concentration. (a) The excess free energy per unit area  $2\pi\Delta F$  and (b) the force per unit area  $\Pi$  between the two surfaces as function of the inter-surface distance w. The salt concentration is  $c_b = 1$ M (solid curve) and  $c_b = 0.25$ M (dots).
- Fig. 12: Adsorption of polyelectrolytes in the low salt regime as calculated from eqs. 28,29. (a) Total amount of monomers adsorbed between the surfaces per unit area  $\Gamma$ , and (b) the average reduced monomer concentration  $\langle \phi^2/\phi_b^2 \rangle$  as function of the inter–surface distance w. The physical values and notations are the same as in Fig. 4. The numerical prefactors of the intermediate profile  $h_3(z,\eta)$  with  $\eta = 3/2$  were used in the calculation. The vertical lines denote the distance where  $w = 2D_1$ .
- Fig. 13: Polyelectrolyte contribution to (a) the interaction free energy,  $2\pi\Delta F_p$  (eq. 30), and (b) the inter-surface force,  $\Pi_p$  (eq. 31), in the low salt regime as function of the inter-surface separation w. Same physical values, notations and units as in Fig. 6. The numerical prefactors of the intermediate profile  $h_3(z,\eta)$  with  $\eta = 3/2$  were used in the calculation of the interaction free energy and forces, and the numerical prefactors of the parabolic profile were used in the calculation of the single surface free energies.
- Fig. 14: Polyelectrolyte contribution to (a) the interaction free energy,  $2\pi\Delta F_p$  (eq. 38), and (b) the inter-surface force,  $\Pi_p$  (eq. 39), in the high salt regime as function of the inter-surface separation w. Same physical values, notations and units as in Fig. 10. The numerical prefactors of the intermediate profile  $h_3(z,\eta)$  with  $\eta = 3/2$  were used in the calculation of the interaction free energy and forces, and the numerical prefactors of the parabolic profile were used in the calculation of the single surface free energies.

Fig. 15: Schematic diagram of the different regimes as function of the charge fraction p and the salt concentration  $c_b$ . Three regimes can be distinguished: (i) the low salt regime  $D_1 \ll \kappa_s^{-1}$ ; (ii) the high salt regime (HS I)  $D_1 \gg \kappa_s^{-1}$  for weak polyelectrolytes  $p \ll (c_b v)^{1/2}$  and (iii) the high salt regime (HS II)  $D_1 \gg \kappa_s^{-1}$  for strong polyelectrolytes  $p \gg (c_b v)^{1/2}$ . The shaded area denotes the region where the polymer interactions are strong enough so that intersurface attraction can be observed. The filled circles correspond to the numerical force-distance profiles of Fig. 6, filled squares correspond to the numerical profiles of Fig. 10 and the filled triangles to the profiles of Fig. 11.

Fig. 16: The effect of irreversible polyelectrolyte adsorption on the interaction free energy. The excess free energy per unit area  $2\pi\Delta F$  is plotted as a function of the inter–surface distance w. The graphs in (a) were obtained by solving numerically the mean field equations 5,48 under the constraint of eq. 46. The solid curve corresponds to the equilibrium interaction free energies and is the same as the solid curve of Fig. 6. The four curves were obtained for the same physical values as in Fig. 5 with p=1 while the total amount of adsorbed monomers was kept at a constant value  $\Gamma_0$ . The different curves correspond to  $\Gamma_0 = \Gamma_{\rm sat} = 0.011 \text{Å}^{-2}$  (dots),  $\Gamma_0 = 2\Gamma_{\rm sat}$  (small dashes),  $\Gamma_0 = 3\Gamma_{\rm sat}$  (long dashes) and  $\Gamma_0 = \Gamma_{\rm sat}/2$  (dot–dash line). The graphs in (b) were calculated from the analytical expressions of the scaling approach (eqs. 51,52).

Fig. 1

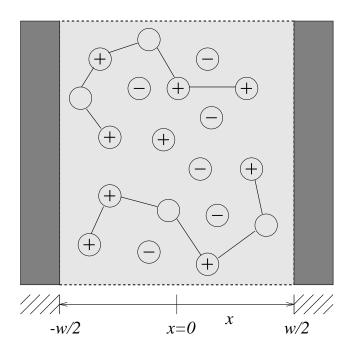
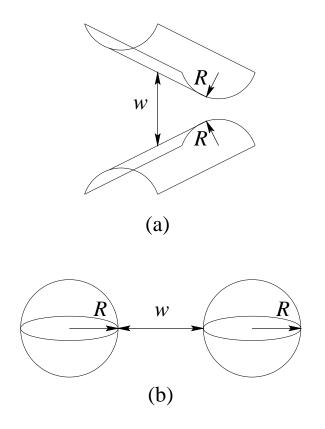


Fig. 2



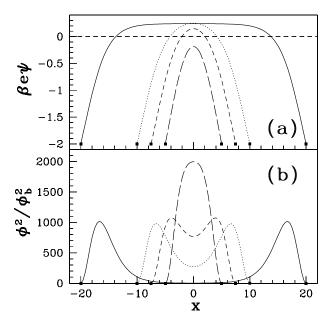
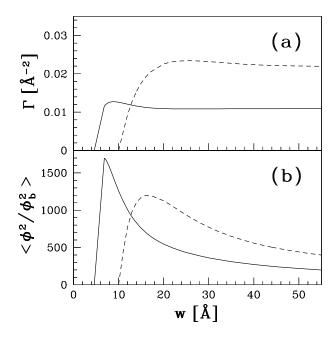


Fig. 4



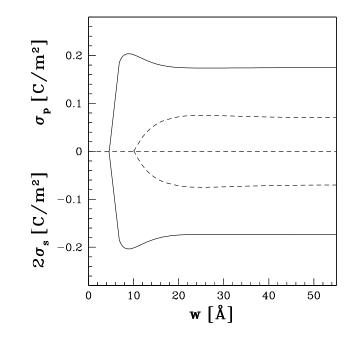
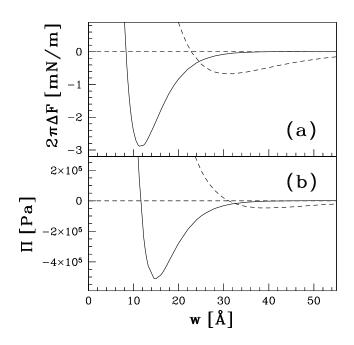


Fig. 6



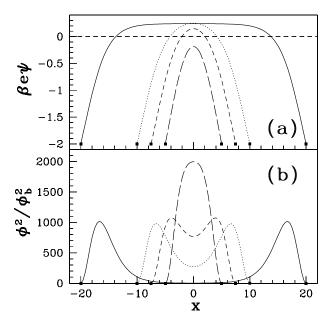
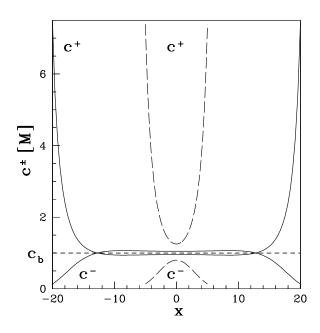


Fig. 8



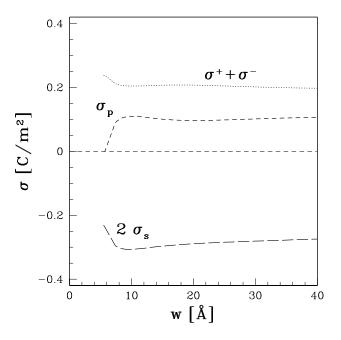
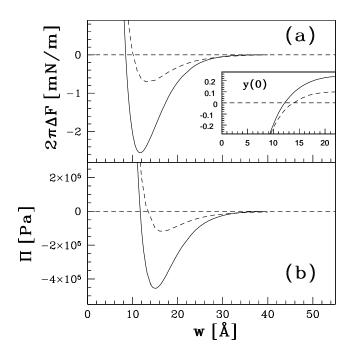


Fig. 10



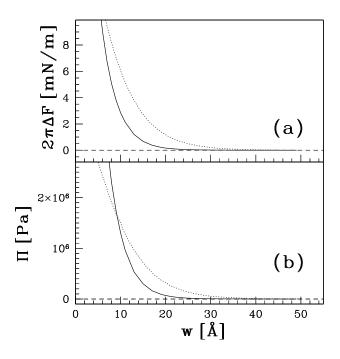
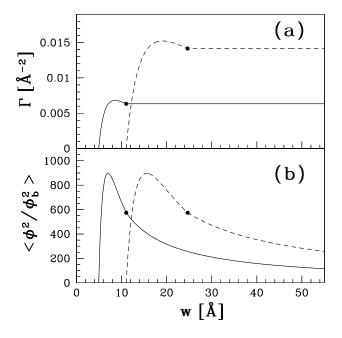


Fig. 12



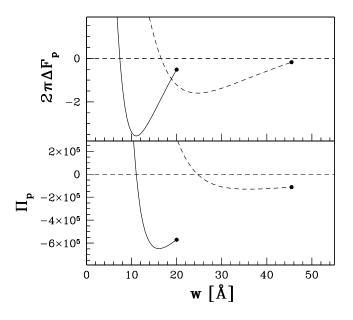
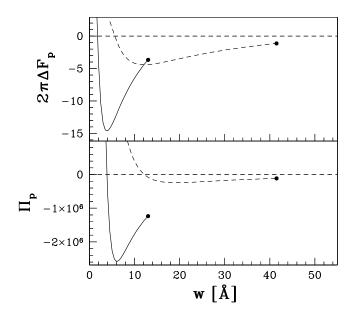


Fig. 14



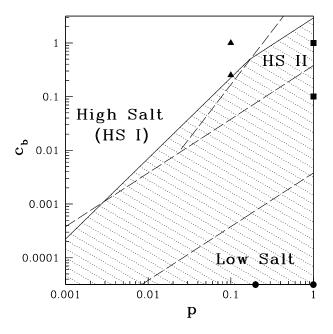


Fig. 16

